

Article

Molecular Dynamics and Nuclear Magnetic Resonance Studies of Supercritical CO₂ Sorption in Poly(Methyl Methacrylate)

Valentina V. Sobornova , Konstantin V. Belov , Alexey A. Dyshin , Darya L. Gurina, Ilya A. Khodov * 
and Michael G. Kiselev

G.A. Krestov Institute of Solution Chemistry, Russian Academy of Sciences, 153045 Ivanovo, Russia

* Correspondence: iakh@isc-ras.ru

Abstract: The study of supercritical carbon dioxide sorption processes is an important and urgent task in the field of “green” chemistry and for the selection of conditions for new polymer material formation. However, at the moment, the research of these processes is very limited, and it is necessary to select the methodology for each polymer material separately. In this paper, the principal possibility to study the powder sorption processes using ¹³C nuclear magnetic resonance spectroscopy, relaxation-relaxation correlation spectroscopy and molecular dynamic modeling methods will be demonstrated based on the example of polymethylmethacrylate and supercritical carbon dioxide. It was found that in the first nanoseconds and seconds during the sorption process, most of the carbon dioxide, about 75%, is sorbed into polymethylmethacrylate, while on the clock scale the remaining 25% is sorbed. The methodology presented in this paper makes it possible to select optimal conditions for technological processes associated with the production of new polymer materials based on supercritical fluids.



Citation: Sobornova, V.V.; Belov, K.V.; Dyshin, A.A.; Gurina, D.L.; Khodov, I.A.; Kiselev, M.G. Molecular Dynamics and Nuclear Magnetic Resonance Studies of Supercritical CO₂ Sorption in Poly(Methyl Methacrylate). *Polymers* **2022**, *14*, 5332. <https://doi.org/10.3390/polym14235332>

Academic Editor: Dagmar R. D’hooge

Received: 10 November 2022

Accepted: 5 December 2022

Published: 6 December 2022

Publisher’s Note: MDPI stays neutral with regard to jurisdictional claims in published maps and institutional affiliations.



Copyright: © 2022 by the authors. Licensee MDPI, Basel, Switzerland. This article is an open access article distributed under the terms and conditions of the Creative Commons Attribution (CC BY) license (<https://creativecommons.org/licenses/by/4.0/>).

Keywords: supercritical carbon dioxide; poly(methyl methacrylate); nuclear magnetic resonance; molecular dynamics

1. Introduction

The study of intermolecular interaction structures in a medium with supercritical state parameters is a complex and multi-stage process where it is necessary to create new methods and improve known ones. The interest in this kind of research is due to both fundamental and practical components. Thus, the use of supercritical fluid technologies is one of the promising ways to create dosage forms with prolonged action as well as new modern medical materials with specified properties [1]. The use of supercritical fluid technology in the sorption processes by highly porous biodegradable polymer materials of medicinal compounds is one of the promising ways to create such medical materials. In such processes, one of the most common solvents is supercritical carbon dioxide (scCO₂) due to the absence of surface tension and high penetrating power. However, the study of such processes is a difficult task since the sorption and swelling of the polymer are usually measured separately using different methods [2–5].

Currently, there are several approaches to the study of changes occurring with polymers during their interaction with supercritical fluids. These include optical reflectometry method [6], silica microbalance [7,8], vibrational spectroscopy [9–15] and some others [16–20]. However, most of these methods are adapted only for polymers in the form of films, and few studies are devoted to the study of powder in volume, which in most cases is close to the actual technological process of production. In this regard, the search for approaches to solving such problems is relevant. The research [21,22] demonstrates that nuclear magnetic resonance (NMR) spectroscopy on ¹³C nuclei is one of the most informative methods to study the kinetics of carbon dioxide (CO₂) sorption into micropores of various aqueous calcium and sodium aluminosilicates of type X, Y, A. It is important to note that the results

are presented in the bulk phase. It is logical to assume that this type of NMR experiment will be informative in the study of the kinetics of sorption of scCO₂ into a polymer matrix. Pressure-controlled NMR spectroscopy is a promising method to study polymers in supercritical CO₂ [23]. In addition, the chemical shift related to CO₂ observed in the polymer-enriched phase can be used to estimate the amount of CO₂ in this phase, which gives access to information about the behavior of polymers in CO₂. In the case of block copolymers, NMR gives a unique idea of the supramolecular structure interfacial region of the core-shell type [24].

There are also many papers devoted to the study of various aspects of adsorption using NMR methods in organic solvents. NMR spectra can be recorded at precession frequencies of various nuclear, but ¹³C NMR spectroscopy is often preferable since it has a wide range of chemical shifts compared to ¹H and, therefore, has a better resolution. Recently, nuclear magnetic resonance with pressure control has been used to study reactions and processes occurring in supercritical solvents [23,25,26]. However, there are no general methodological techniques described in the literature to study the processes of sorption and swelling of the polymer matrix in volume at supercritical solvent parameters at the moment.

We have developed and tested a method to obtain kinetic characteristics of polymer sorption and swelling in supercritical CO₂ based on ¹³C NMR spectroscopy and molecular dynamic (MD) modeling. The approach presented in this paper is based on NMR spectroscopy methods applied to the assessment of changes in the characteristics of the polymer matrix in the scCO₂ medium and provides a new way to measure CO₂ sorption and swelling in the polymer volume simultaneously. Polymethylmethacrylate (PMMA) was chosen as a model compound for testing ¹³C NMR spectroscopy approaches. This choice is due to the large volume of experimental studies of the PMMA-CO₂ system presented in the literature at various state parameters. In particular, in the papers [17,27] the authors studied the sorption of CO₂ in PMMA at 32–65 °C and pressure up to 10 MPa. Kamiya investigated the sorption of CO₂ in PMMA in the range of 35–200 °C and with pressure up to 6 MPa [28]. Rajendran and co-authors investigated the sorption behavior of CO₂ in PMMA at 50, 65 and 80 °C and pressures up to 23.8 MPa [29]. Vogt et al. investigated the sorption of CO₂ in PMMA 60 and 100 °C and pressures up to 12 MPa [30]. Shie and Liu studied sorption and CO₂/PMMA interactions at temperatures of 32, 42 and 52 °C and pressures up to 35 MPa [31]. It is worth noting that the NMR method is rarely used in practice due to the need to use isotope-labeled ¹³C samples. However, if a certain density of a supercritical fluid based on CO₂ is achieved, the sensitivity of the ¹³C NMR experiment may be sufficient to register spectra with a good signal-to-noise ratio. This circumstance was the reason for the parameters of performing kinetic NMR experiments, namely $\rho_{\text{CO}_2} = 1.3 \cdot \rho_c$ ($\rho_c = 467 \text{ kg/m}^{-3}$) of critical density. On the other hand, the impregnation process should be sufficiently slow in the NMR time scale to be able to register the observed sorption and swelling effects based on ¹³C NMR spectroscopy. The feature of NMR approaches is that the time scales of the physicochemical processes studied are limited to minutes and hours. However, the initial stages of sorption processes occur at the peak and nanosecond scales. From this point of view, the NMR study will be well complemented by MD modeling.

It is good practice to use computer simulation approaches in addition to experimental techniques when investigating complex processes. In this work, the process of sorption of supercritical carbon dioxide into the matrix of poly (methyl methacrylate) is studied by the method of classical molecular dynamics. Although the time and length scales of MD simulations are limited to a few nanoseconds and nanometers and significantly differ from experimental scale, MD is a useful and powerful tool for explaining phenomena observed in the experiment and at the same time for investigating systems at the molecular level. Previously, systems containing PMMA and scCO₂ were studied by MD [32–35], and it was shown that computer simulation allows obtaining molecular insight on swelling behavior of the polymer and obtaining tendencies sufficiently agreed with the ones observed in experiment.

2. Materials and Methods

2.1. NMR Experiments and Methodology

To measure the NMR spectra of ^{13}C at supercritical parameters of the CO_2 state, a system to create and maintain high pressure in real time was used (see Figure 1), based on a unique scientific installation “Fluid Spectrum” (<https://ckp-rf.ru/usu/503933/> accessed on 6 December 2022) of G.A. Krestov Institute of Solution Chemistry of the Russian Academy of Sciences. The installation connects a high-pressure cylinder (Figure 1 pos. 1) containing carbon dioxide gas, with high-pressure NMR cell due to a high-pressure capillary. Filling and emptying high-pressure NMR cell is possible because of the system of taper seal valves (Figure 1 pos. 3, 6). Pressure monitoring is implemented using a pressure gauge (Figure 1 pos. 2) and electronic pressure transmitters (Gems™ Sensors&Controls, Basingstoke, UK) (Figure 1 pos. 5), a pressure adjustment in high-pressure NMR cell is carried out by means of a manual press (Figure 1 pos. 4). The accuracy of maintaining the pressure was ± 0.05 MPa.

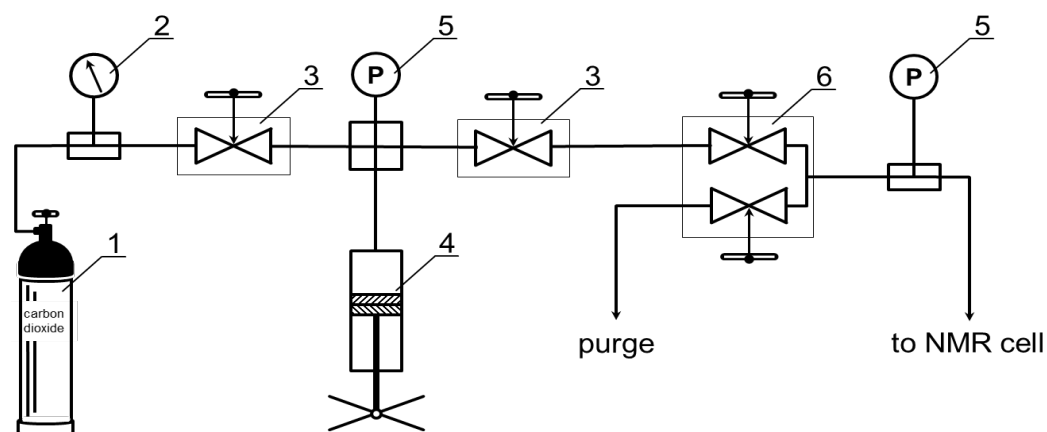


Figure 1. Scheme of the apparatus for producing and maintaining high-pressure for NMR measurements in carbon dioxide media, where 1 is a cylinder with carbon dioxide, 2 is a pressure gauge, 3, 6 are taper seal valves for filling (**upper**) and purging (**lower**), 4 is a manual press, 5 and 8 are electronic pressure transmitters, and 9 is a high-pressure NMR cell (see. Figure 2).

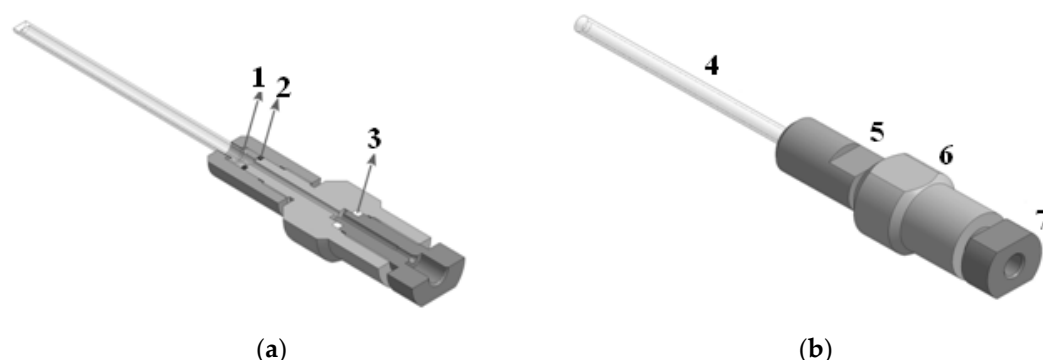


Figure 2. (a) High-pressure NMR cell (cross section): 1 is a capillary inlet seal (Teflon, Chemours, Wilmington, DE, USA), 2 is an ampoule seal (MVQ Silicones GmbH, Weinheim, Germany), 3 is a compensating gasket (Caprolon—polyamide, Shik Polymers, Moscow, Russia) (b) High-pressure NMR cell (full view): 4 is a high-pressure tube (synthetic single crystal sapphire Al_2O_3), 5 is a tube holder (D16T, Metatorg, Ivanovo, Russia), 6 is an input port (D16T, Metatorg, Ivanovo, Russia), 7 is a capillary inlet high-pressure (D16T, Metatorg, Ivanovo, Russia).

High-pressure NMR cell (Figure 2b pos. 4) [36–38] is a single crystal sapphire tube of high-pressure production (Daedalus Innovations, Aston, Pennsylvania, USA). The small size of the ampoule, which has an inner diameter of 3 mm, an outer diameter of 5 mm

and a total length of 87 mm, allows it to work at pressures up to 30 MPa. The sapphire ampoule is equipped with an upgraded [39] cell fixation system (Figure 2b pos. 5), capillary mounts (Figure 2b pos. 6, 7) and sealing elements (Figure 2a pos. 1, 2, 3) to supply CO₂ continuously. The temperature range of the cell is limited by the temperature range of the NMR spectrometer sensor.

NMR spectra were obtained using a Bruker Avance III 500 (Bruker Co., Karlsruhe, Germany) spectrometer equipped with a 5 mm Bruker TBI probe. The temperature was controlled by a VT-2000 prefix (Bruker Co., Karlsruhe, Baden-Württemberg, DE) with a Bruker BCU cooling unit (Bruker Co., Karlsruhe, Germany), the air consumption was 535 L/hour. Temperature calibration was carried out using a standard K-type thermocouple (Bruker Co., Karlsruhe, Germany). ¹H NMR spectra of methanol were used as a method of temperature verification and calibration [40].

Polymethylmethacrylate (PMMA) powder was used as a sorbent (CAS No: 9011-14-7) of the Aldrich™ (Sigma–Aldrich, Moscow, Russia). The impregnation was carried out in a carbon dioxide environment (CAS No: 124-38-9) of the primary standard, GOST 8050-85 (CO₂—99.995%, H₂O— < 0.001%) produced by Linde Group Russia (Balashikha, the Linde Group, RF). All substances were used without additional purification.

¹³C NMR spectra of scCO₂ were obtained using a pulse program included in the software package of the TopSpin 3.6.1 for NMR spectrometer. The spectra were measured at a temperature of 50 °C and a pressure of 250 bar in the spectral range of 284 ppm to reduce the statistical error, 1024 scans were performed to obtain each spectrum, followed by averaging. A total number of 93 NMR ¹³C spectra were obtained with a fixed time interval between them equal to 90 min.

2.2. NMR Experiment Parameters Selection

To select the parameters of the experiment, we turned to the experimental data on the kinetics and sorption of PMMA in CO₂, given in the literature [41]. As shown in [41] CO₂ is better sorbed by the polymer matrix with increasing pressure. Thus, to increase the sensitivity of the ¹³C NMR experiment, a pressure over 20 MPa should be chosen. At the same time, the dependence of the sorption logarithms on pressure is demonstrated by the presence of two sorption modes [41].

The first sorption mode is observed at relatively low pressure up to 10 MPa and is characterized by low values of sorption intensity and capacity. The opposite mode is observed for pressure above 10 MPa and is characterized by relatively high values of capacitance and intensity, which makes it preferable for ¹³C NMR studies. However, when selecting the temperature values, some ambiguities arose. On the one hand, the sorption intensity in the high-temperature regime increases with increasing temperature, on the other hand, the sorption capacity decreases by an order of magnitude, which, of course, can significantly reduce the sensitivity in the ¹³C NMR experiment. With this in mind, when setting up the ¹³C NMR experiment, a temperature of 50 °C was used. It is due to a reduction in the duration of the NMR kinetics experiment from two weeks to one and the possibility of observing the process in a reasonable time. It is worth noting that the obtained parameters of in situ measurement of sorption and swelling in the volume of polymer powder can be used to optimize the production processes of polymer impregnation in supercritical liquids.

2.3. Computational Details/MD Method

Each polymer chain first contained 100 monomers; then 108 chains were used to construct a three-dimensional structure with an initial density of 1000.0 kg/m³. The MD simulations were conducted in graphics processing unit-accelerated GROMACS v5.0.7 [42]. In our previous work [33], we described the methodology of bulk PMMA simulation with the Optimized Potentials for Liquid Simulations-All Atom (OPLS-AA) force field in detail [43]. In the current study, we used the same Lennard-Jones (LJ) and partial atomic charge parameters as in [33]. For carbon dioxide, we used the model developed

by Z. Zhang and Z. Duan [44]. To calculate the cross site-site interactions, we used the geometric mean mixing rule for both LJ parameters. The temperature (323 K) and pressure (25 MPa) were controlled by a Nose'-Hoover thermostat [45,46] and a Parrinello-Rahman barostat [47], respectively. In Figure 3, time dependence of pressure and temperature during the simulation process is shown. The leap-frog integrator has been used for solving the equations of motion [48]. The cutoff radius was set to 1.5 nm for all the interactions. In the case of long-range electrostatic interactions, we used a particle mesh Ewald [49,50] with a grid spacing of 0.25 nm and an interpolation order of four. The constraints were implemented using the LINear Constraint Solver (LINCS) algorithm, to preserve the correct bond lengths [51].

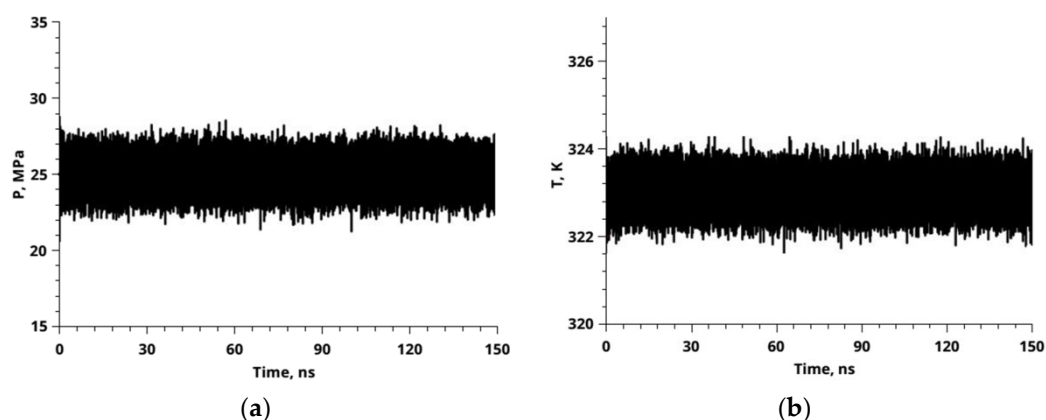


Figure 3. Time dependence of pressure (a) and temperature (b) during simulation process for 150 ns with a time step of 2 fs. These graphs confirm the reliability of the use of the barostat and thermostat and the absence of parameters of state (temperature in K and pressure MPa) changes throughout the duration of the simulation.

A sample of PMMA (with linear dimension of about 16 nm) consisting of 108 chains equilibrated at 323 K and 0.1 MPa was placed in the center of a cubic cell with periodic boundary conditions and immersed in 242,522 CO₂ molecules equilibrated in advance at 323 K and 25 MPa. After the energy minimization, we performed production run simulations in the NpT ensemble for 150 ns with a time step of 2 fs. Data for analysis were collected every 0.5 ps. The final length on the cubic simulation cell was 30.36 nm.

2.4. RRCOSY Analysis

The basic principle of using the ARCOS method is based on inverting relaxation curves with one or more relaxation distributions [52,53], according to Equation (1):

$$L(g(-R_n)) = \int g(R_n) \exp(R_n t) dR_n \quad (1)$$

where $g(R)$ is the relaxation velocity distribution function ($R_n = 1/T_n$) which is defined only for $R > 0$. In practice, when conducting NMR experiments, the inverse Laplace transform is used. In particular, the distributions of the inverse transformation $L(T_1)$ for the spin-lattice relaxation time T_1 and $L(T_2)$ for the spin-spin relaxation T_2 , with experimental noise $E(t)$, are determined by Equations (2) and (3):

$$M_{SR}(t) = l(T_1) \left[1 - \exp\left(\frac{-t}{T_1}\right) \right] dT_1 + E(t) \quad (2)$$

$$M_{CPMG}(t) = l(T_2) \exp\left(\frac{-t}{T_2}\right) dT_2 + E(t) \quad (3)$$

These equations are used to obtain one-dimensional distributions of relaxation times. In papers [54] two important features of conducting experiments with the Laplace trans-

form were identified. The first feature is that the Laplace transform is noise-resistant; in other words, a small random error has little effect on the results after the transformation. The second feature is that the inverse Laplace transform is very unstable and needs additional regularization mechanisms. The description of algorithms for applying the Laplace transform to discrete data obtained during measurements is given in the papers [52,55].

It is worth mentioning the main feature to be characteristic of the inverse Laplace transform when constructing a two-dimensional correlation map of relaxation times. Distributions $1 - \exp^{-t/T_1}$ and \exp^{-t/T_2} may have several dependencies on the relaxation time in 2D NMR spectroscopy of the inverse Laplace transform which leads to a multidimensional spectroscopic image. In particular, the reverse Laplace transform spectroscopy used in this work T_1 - T_2 Relaxation-Relaxation Correlation Spectroscopy (RRCOSY) [53,56] combines two pulse sequences. One of them is used by restoring the longitudinal magnetization after saturation of the NMR signal encoded in τ_1 , and the CPMG sequence (Carr-Purcell-Meiboom-Gill) encoded in τ_2 . Given the notation, the inverse Laplace transform in this case will take the form:

$$M_{RRCOSY}(\tau_1, \tau_2) = \iint (1 - \exp\left(\frac{-\tau_1}{T_1}\right) \exp\left(\frac{-\tau_2}{T_2}\right) L(T_2, T_1) dT_1 dT_2 + E(t) \quad (4)$$

where $E(t)$ represents Gaussian additive noise.

Numerical integration according to Equation 4 is a certain transformation algorithm that requires constant adjustment of the selection of parameters, which in itself is a complex and time-consuming process. However, with the advent of the fast Laplace transform created by Venkataraman and co-authors [57], the condition has changed. Venkataraman's algorithm significantly simplifies spectrum analysis and gives the opportunity to identify narrower areas of correlation. Since NMR relaxation processes are often first-order processes, it is the inverse Laplace transform (2D ILT) that translates data from the time domain of the experiment into the corresponding correlation spectra of relaxation time values. Information about whether there is more than one distinct mode or peak in two-dimensional relaxation time spectra can provide direct data on sorption sites and their number. In the literature, it has been shown [58–61] that time domain analysis of multidimensional 2D ILT relaxation experiments, such as RRCOSY, can quantify exchange parameters quite efficiently.

However, obtaining information about exchange processes by directly applying the inverse Laplace transform equation is often very difficult, since it is extremely sensitive to the initial experimental data in the case of two peaks in the 2D ILT spectra. In practice, there are two approaches to obtaining qualitative data for the selection of processing parameters based on the magnitude and shape of the peaks [62,63], one with additional modeling, and the other without it. Thus, in the approach adapted to describe the processes of polymer matrix sorption, a model of relaxation exchange main processes in the sample is proposed with subsequent adjustment of the parameters of this model to achieve the best match with 2D ILT data [60]. The minimum R^2 factor of the least squares method is chosen as the criterion of compliance. Such a model is a special case of multi-node relaxation where only two nodes are considered. This model was first proposed and described in detail by McConnell in 1958 [64].

A two-node model can be obtained from a kinetic description of the change in the magnetization balance with time for a two-position exchange:

$$d/dt \begin{bmatrix} M_a - M_a^{eq} \\ M_b - M_b^{eq} \end{bmatrix} = \begin{bmatrix} -R_a - k_a & k_b \\ k_a & -R_b - k_b \end{bmatrix} \begin{bmatrix} M_a - M_a^{eq} \\ M_b - M_b^{eq} \end{bmatrix} \quad (5)$$

where R_a and R_b are the proper relaxation rates, longitudinal or transverse for two sites (a and b), and k_a and k_b are the exchange rate coefficients that characterize the transfer from site a to b and from site b to a , respectively. M_a and M_b represent the magnetization

of specific exchange nodes, and M_a^{eq} and M_b^{eq} provide the magnetization values of nodes that are in thermal equilibrium with the applied field.

The magnetization balance equation in formula (5) can be written in a more compact form:

$$dM/dt = AM \tag{6}$$

where M is a two–element magnetization vector of nodes and the matrix A contains a combination of the corresponding relaxation and exchange coefficients:

$$A = [R + K] = \begin{bmatrix} -R_a - k_a & k_b \\ k_a & -R_b - k_b \end{bmatrix} \tag{7}$$

The presented model describes the evolution of magnetization in the delay regions of the pulse sequence, taking into account the relaxation conditions for transverse or longitudinal processes, depending on the interval. The initial conditions for each interval in the pulse sequence are provided by radio frequency pulses preceding the evolution of magnetization. The fitting is performed by adjusting the parameters in the matrix A (Equation (7)) using the least squares method for the pulse sequence so that the model predictions coincide with the experimental data in the best way. The analytical solution of Equation 6 was obtained and described in detail for several 2D ILT pulse sequences, including for RRCOSY [58,59].

A useful result that follows from the solution of the presented equations is expressed in the ability to predict peak amplitudes of 2D ILT spectra using the so-called peak matrix P [59].

The expression for matrices P for the RRCOSY pulse sequence (Figure 4) is written as:

$$P_{T_1 T_2} = 2 \left[U_2^{-1} \exp([R_1 + K]t_1) M(0) \right]^\circ [1_{1 \times N} U_2]^T \tag{8}$$

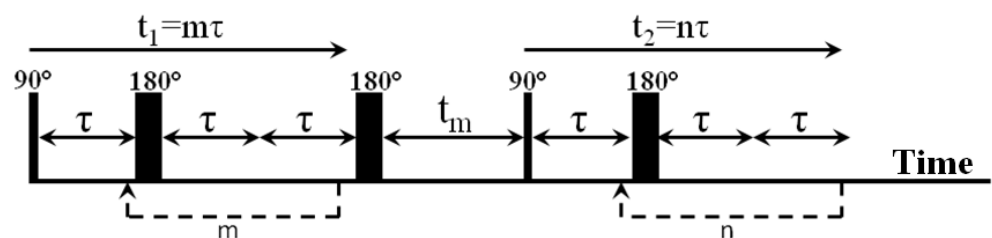


Figure 4. The RRCOSY pulse sequence used in the experiment consisting of two 90° and three 180° radio frequency pulses, where t_1 is the time of the indirect encoding period, t_2 is the time of the detection period, t_m is the mixing time, m and n are the numbers of echo times in the encoding periods.

In expression 8, the eigenvectors $U_{1,2}$ are a matrix of eigenvectors obtained from the matrix $R_{1,2} + K$, $M(0)$ is the initial magnetization for the sequence, which in practice is usually equilibrium magnetization, t_1 and t_m are given by the time parameters of the pulse delays, and $1_{\chi N}$ is an N –element string vector. The symbol \circ represents the element-wise multiplication (Hadamard multiplication) of the matrix between two multipliers. A detailed description and properties of this equation are presented in the paper [59].

Another method, the so-called data reconstruction method, aims to directly calculate the unknown function $L(t_2, t_1)$ directly from the equation for M_{RRCOSY} . At the first stage of $M_1 \times M_2$ samples of $t_1 \times t_2$ times and $N_1 \times N_2$ samples of $T_1 \times T_2$ relaxation times, problem (1) is discretized as:

$$(K_2 \otimes K_1) f + e = s \tag{9}$$

where $K_1 \in R^{M_1 \times N_1}$, $K_2 \in R^{M_2 \times N_2}$ represent the discretized exponential kernels of the integral equation, and \otimes —binary product of matrices of arbitrary size (Kronecker product) [65,66], $s \in R^{M_1 \cdot M_2}$ —discrete vector of experimental noisy data, $f \in R^{N_1 \cdot N_2}$ —distribution re-ordering vector, and $e \in R^{M_1 \cdot M_2}$ —vector with sampled noise. Within this approach, the

multiparametric Tikhonov regularization problem is numerically solved to minimize the functions of the type:

$$\min_{f \geq \uparrow} \left\{ \|(K_2 \otimes K_1)f - s\|^2 + \sum_{i=1}^N \lambda_i (Lf)_i^2 \right\} \quad (10)$$

where $\|(K_2 \otimes K_1)f - s\|$ —norm L_2 , $L \in R^{N \times N}$ —discrete Laplace operator, λ_i —regularization parameters, from $i = 1, \dots, H$. This numerical solution is an iterative procedure where at each iteration step, suitable values of λ_i are determined by imposing the condition that all nonzero products of $\lambda_i (Lf)_i^2$ have the same constant of values (Uniform PENalty principle) and an approximate distribution is obtained by solving an equation of form 10 using the Newton projection method. This approach was used in the work.

3. Results

3.1. Sorption of CO₂ from NMR Experiment

Having determined the parameters of the ¹³C NMR experiment as 50 °C and 25 MPa, when developing the methodology for obtaining physico-chemical characteristics, it becomes necessary to find “markers” or “fingerprints” of the sorption and swelling processes of the PMMA system/CO₂. It should be noted that ¹³C NMR signals of PMMA carbons are not observed in high-resolution NMR spectroscopy. This is due to the fact that without rotating the sample at a magic angle, the spectrum of a solid-state sample takes several hundred kilohertz and is leveled during mathematical processing of the spectrum. Thus, the value of the ¹³C chemical shift observed in the experiment for CO₂ is an average sum of the adsorbed polymer matrix and free CO₂. This picture is the opposite in comparison with the study of CO₂ sorption by activated carbon fiber using ¹³C spectroscopy [67]. The overlap of the π -electrons of the carbon fiber leads to a sufficiently noticeable effect of screening the ¹³C nuclei for adsorbed CO₂ molecules [68], which can be seen in the form of an additional wide signal with a shift to a strong field. It should be noted that such an effect is characteristic of activated carbon fiber, while for other systems, such as polymer matrices, in practice such changes in chemical shifts are not observed. Thus, the only possible way to obtain “markers” characterizing the processes of CO₂ sorption into the polymer matrix of PMMA, as well as its swelling, is to change the spectral characteristics of one signal: resonance frequency, half-width at half-height and integral intensity.

To solve this problem, a series of ¹³C NMR experiments was carried out with subsequent processing of the spectral contour of the lines of resonant CO₂ signals. A similar methodology is used for the analysis of vibration spectra [69]. In total number 93 ¹³C of the spectrum were obtained with a fixed time interval between them equal to 26 min. However, unlike vibration spectra, where the pseudo-Voigt function is used, in practice, the Lorentz function is used to process the spectral contour of the lines of resonant signals of ¹³C NMR spectra in liquids [70,71]. The main feature of the methodology used is that, unlike thin films, the work takes place directly with the powder, which is the best approximation to the conditions of polymer production.

Figure 5 shows the ¹³C NMR spectra of free CO₂ gas and CO₂ adsorbed into the polymer matrix of PMMA at P = 25 MPa and T = 323.15 K. When analyzing the obtained ¹³C NMR spectra (Figure 5), only two signals can be seen. One of which is a triplet in a weak field and belongs to deuterated benzene sealed in an ampoule, used to calibrate the resonant frequency of 128.39 ppm, and the second located in a strong field is a singlet—CO₂.

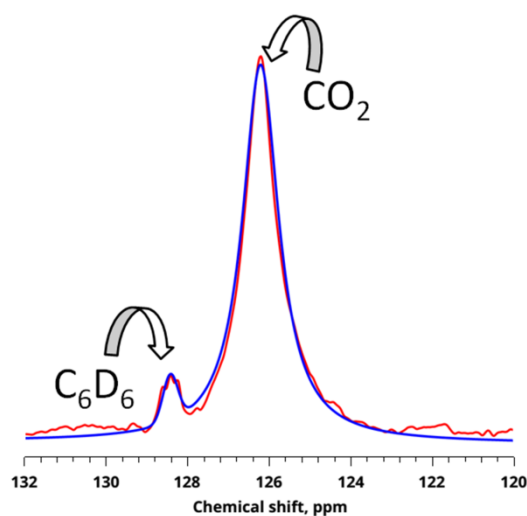


Figure 5. An example of quality of approximation of the spectral contour of the ^{13}C NMR resonance signals of CO_2 and standard C_6D_6 (red line) by Lorentz-like profiles (blue line) using pseudo-Voigt functions.

The magnitude of the chemical shift of the resonance peaks for CO_2 in PMMA was the same as for the volume value ($\delta = 126$ ppm) within the experimental error and the line full width at half maximum (FWHM) in these adsorbents ($51 \text{ Hz} \leq \text{FWHM} \leq 72 \text{ Hz}$) was slightly larger than for the volume (FWHM = 51 Hz in the volume of CO_2). As discussed below, this effect is related to the peculiarities of sorption processes. Despite the fact that at the moment there are very few studies devoted to the sorption of CO_2 into the polymer matrix by the ^{13}C NMR method, there are several studies where the dynamics and local structure of several porous materials, such as zeolites, are analyzed [72] and activated carbon fiber [67]. As shown [22], for some zeolites, the difference in the magnitude of the chemical shift for the molecules of the bulk gas and adsorbed to the surface was 0.7 ppm in a higher field, which is also observed within the margin of error for activated carbon fiber. This suggests that the adsorbed CO_2 molecule in the micropores of zeolites and fibers weakly interacts with the pore wall in these adsorbents. A similar situation was observed for our samples. The magnitude of the change in the chemical shift was only 0.2 ppm in the direction of a strong field, which indicates that PMMA is inferior in its sorption properties to zeolites or carbon fiber. However, the fact that changes in the chemical shift occur in the direction of a strong field also indicates that the change in the chemical shift of ^{13}C CO_2 signals in the gas phase is due to sorption processes into the polymer matrix. When studying sorption processes of CO_2 into a polymer matrix, unlike carbon fiber, we do not observe broad signals in the 123 ppm region because the specific interaction of the surface of PMMA micropores and CO_2 molecules with π electrons is much weaker compared to carbon fiber or absent altogether. For CO_2 molecules enclosed in micropores, equilibrium has been achieved between adsorption and desorption of CO_2 molecules. Therefore, by analogy with the results concerning the CO_2 sorption of carbon fiber, it is logical to assume that the observed value of the chemical shift ^{13}C for limited CO_2 molecules is determined by the weighted average value of the chemical shift between CO_2 adsorbed on the surface of the PMMA and CO_2 co-existing in the micropore space and/or in the space near the entrance to the micropores.

Figure 6 shows a graph of the dependence of the chemical shift values of ^{13}C NMR scCO_2 on time. For clarity, dependence is presented in the hourly time scale. The chemical shift is responsible only for the sorption process, since during swelling the polymer does not change its magnetic environment and, accordingly, does not significantly contribute to the observed chemical shift of CO_2 . To describe the process of CO_2 sorption in the pores

of the PMMA polymer matrix, this dependence was approximated by the function that in practice proved to be the most accurate for describing the processes of CO₂ sorption [73].

$$\delta_C = \delta_e + \delta \exp(-kt) \quad (11)$$

where δ_C is the value of the chemical shift of the resonant CO₂ signal sorbed at time t , δ_e is the value of the chemical shift of the resonant CO₂ signal sorbed at saturation, k is the sorption constant, δ is the multiplier corresponding to the difference between the value of δ_e and the initial value of δ_C (at time $t = 0$).

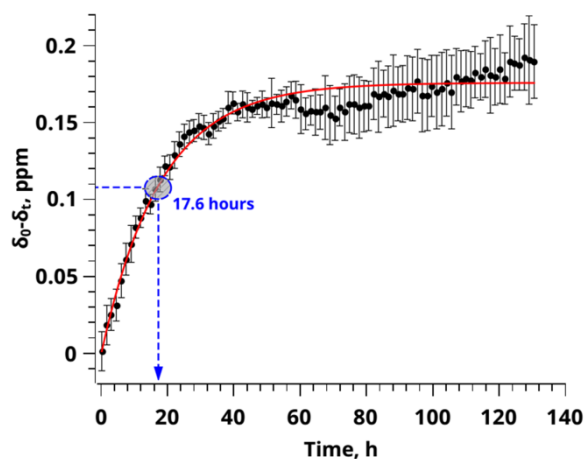


Figure 6. A graph of the change dependence in the parameter of the chemical shift of the ¹³C CO₂ signal on time, approximated by a one-exponential model. Where δ_0 is the value of the chemical shift of the ¹³C CO₂ signal at the initial time, δ_t is the value of the chemical shifts of the ¹³C CO₂ signal at observation time t . The blue circle on the graph indicates the correlation time of this sorption process, defined as the reciprocal of the rate constant of the sorption process (k).

As can be seen from Figure 6, the use of this mathematical model made it possible to approximate the experimental curve with high accuracy ($R^2 = 0.961$). This confirms the predominance of the main process of CO₂ sorption on the chemical shift value. The application of the proposed mathematical model made it possible to establish the rate constant of the sorption process (k), the value being 0.057 h^{-1} , as well as the value of the equilibrium value of the chemical shift of 126.023 ppm (see Figure S1). The correlation time of the process was determined in accordance with the value of the rate constant $t_c = 1/k$ and was $t_c = 17.6 \text{ h}$.

Using the values of the half-widths and integral intensities, it is possible to construct a kinetic dependence to determine the sorption parameters (Figure 7a,b). However, unlike the chemical shift, the integral intensity and half-width values can be influenced by other kinetic processes occurring with the polymer matrix during sorption. According to the literature data, such a process in the PMMA scCO₂ system is swelling [20,74]. To test the hypothesis about the possibility of sorption processes in the analysis of kinetic dependences of half-widths, two mathematical models were used, by analogy with Equations (12)–(13).

$$\Delta_C = \Delta_e + \Delta \exp(-kt) \quad (12)$$

$$\Delta_C = \Delta_e + \Delta_1 \exp(-k_1 t) + \Delta_2 \exp(-k_2 t) \quad (13)$$

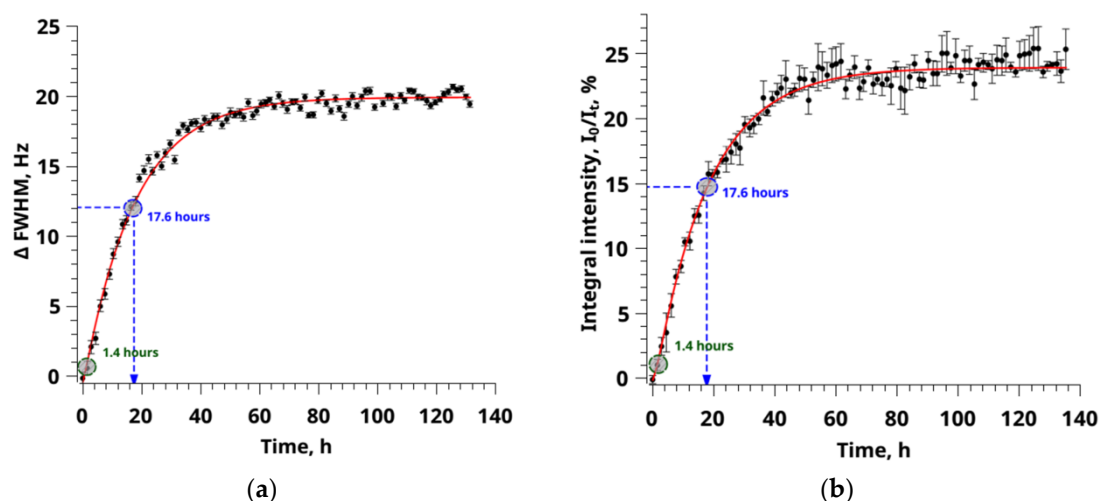


Figure 7. (a) A graph of the change dependence in the signal width parameter at the half-height of the ^{13}C CO_2 signal on time, approximated by a two-exponential model. Where $\Delta\text{FWHM} = \text{FWHM}_0 - \text{FWHM}_t$, where FWHM_0 and FWHM_t are the half-widths of the signals at half-height at the initial time and observation time t , respectively. (b) A graph of the change dependence in the parameter of the integral intensity of the ^{13}C CO_2 signal on time, approximated by a two-exponential model. Where I_0 and I_t are the values of the integral signal intensity at the initial moment of time and the observation time t . The blue and green circles on the graphs show the values of the correlation times of the sorption and swelling processes, respectively.

Applying the equations, a fairly accurate approximation of the experimental data of the theoretical curve of values $R^2 = 0.985$ was obtained. Moreover, these velocity constants and correlation times are somewhat overestimated compared with the values obtained from the analysis of chemical shifts. However, the use of a two-exponential model allowed not only to improve $R^2 = 0.986$ but also to confirm the existence of the second faster process. Its speed is an order of magnitude higher than the sorption rate of 0.714 h^{-1} and the correlation time is an order of magnitude less than $t_c = 1.4 \text{ h}$, respectively. Moreover, the advantage of the proposed data analysis is the use of the values of constants obtained from the analysis of chemical shifts to approximate the data of integral intensity and half-widths in a two-exponential model. This method is possible due to the different nature of the parameters observed in the experiment.

Even though, at first glance, the approximation by a two-exponential model does not show significant improvements, this method allows us to capture such a slight effect of the polymer matrix swelling on the observed experimental parameters (Figure 7). The approach of analyzing experimental data by approximating mathematical models has a significant drawback, i.e., it is impossible to obtain unambiguous experimental evidence of the existence of more than one sorption process from a direct ^{13}C NMR experiment.

3.2. Sorption of CO_2 from NMR Experiment—2D RRCOSY

It is impossible to isolate the characteristic type of molecules by analyzing only the values of chemical shifts or integral intensities of ^{13}C CO_2 . For further analysis of the results obtained, additional methods are required that can be used to justify the choice of a kinetic model to interpret experimental data. The analysis of the literature has shown that at the moment there is no reliable, universal technique to study the adsorption characteristics of a polymer matrix with a saturated fluid. In addition, sorption measurements based on chemical shift analysis will be very limited in terms of multicomponent systems inside polymer pores due to the wide overlapping lines associated with each component. The approach proposed in this paper is based on the analysis of the characteristic relaxation times of NMR. This approach is spared from these kinds of problems. Moreover, as shown in [75], the ratio of spin–lattice to spin–spin relaxation times (T_1/T_2) is directly related to

the activation energy of desorption. Therefore, when developing this method, relaxation times were taken as the main parameters of the sorption characteristic.

One of the effective methods for distinguishing the types of molecular lability of CO₂ in a material including in a polymer matrix is RRCOSY spectroscopy. The RRCOSY technique makes it possible to observe correlations of T₁-T₂ relaxation times by means of a two-dimensional inverse Laplace transform. The data obtained using RRCOSY spectroscopy represent populations of certain amplitudes which are generated due to various physical regions of mobility in the material and form regions (sites).

Based on Venkataraman's work on the direct model (in Section 2.4), proprietary algorithms were implemented that allow not only to build a spectrum but also to integrate the obtained correlation regions. The two-dimensional correlation map obtained based on the developed method is shown in Figure 8.

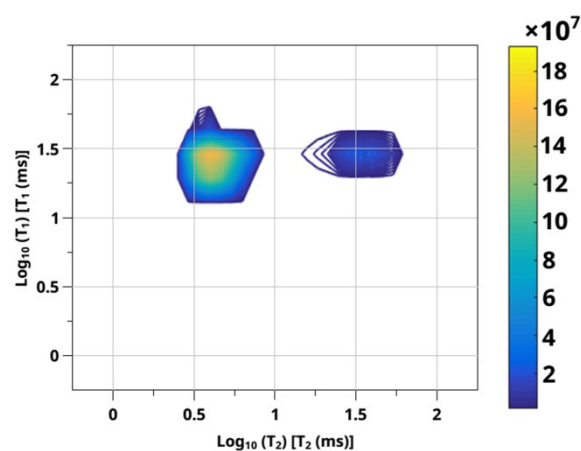


Figure 8. Two-dimensional correlation map obtained on the basis of the developed method. The ordinate and abscissa show the values of the logarithms of the relaxation times T₁ and T₂ spin–lattice to spin–spin relaxation times, respectively, while the sites in the spectroscopic image correspond to free solvent scCO₂ (left) and impregnated into the polymer matrix (right).

Figure 8 shows that two sites are present on the graph and although two T₂ values have been identified, only one T₁ value is observed. Two-dimensional ILT, predictable by the elements of the matrix of the analytical model [76], demonstrates four peaks of different amplitudes corresponding to the eigenvalues of the solution matrix. It corresponds to two peaks “diagonally” and two peaks of exchange. Diagonal peaks represent internal relaxation and internal relaxation weighted by exchange, which corresponds to the peaks with the shortest T₁, T₂ and the longest T₁, T₂ at the bottom left and top right, respectively. The other two peaks are exchange peaks: with a long relaxation time T₁ which is associated with a short relaxation time T₂, and a corresponding short time T₁ associated with a long T₂. The results of the 2D ILT experiment clearly show two main peaks: one is located at the longest values T₁ and T₂, and the second is the exchange peak located at the long values T₁ and short T₂. At the same time, the other two peaks are not visible. The presence of an exchange peak indicates that mixing between the populations of spin states occurs on the time scale of longitudinal relaxation in the system under study [77–80]. The exchange process averages T₁ relaxation processes. Consequently, the internal values of T₁ are difficult to isolate, and one T₁ value is observed. However, it is still possible to provide internal T₂ values using the direct data analysis method. Using a specially developed program that allows the construction and numerical integration of the obtained 2D ILT spectra, the values of integral intensities were obtained, and they amounted 0.15 to 14.72. Thus, the integral intensity of the non-diagonal peak is lower than the diagonal one. To interpret the results from a physicochemical point of view, it is necessary to understand that sites are physical areas of different mobility of scCO₂ in the material to manifest themselves in a population of a certain amplitude and intensity. These two-dimensional experiments

provide information about diffusion and trends in relaxation times which allow for a better understanding of the scCO₂ state in the polymer matrix. It is worth noting that one of the populations, which manifests itself as a non-diagonal peak, is located within the parity line $T_1 = T_2$, where data representing sites of the free solvent scCO₂ may appear. It is known from the literature that the farther the population is from the parity line, the more the rotational mobility of molecules is limited [56], and the closer the sites are to the parity line, the freer the rotational mobility. Thus, there are two pronounced sites in the polymer matrix that are physically responsible for free CO₂ molecules and impregnated into the polymer matrix, numerical integration of these sites showing a significant excess of the concentration of CO₂ in the polymer matrix over the free ones.

3.3. Sorption of CO₂—MD Simulation Results

Different mobility of carbon dioxide molecules is also observed in the simulated system. Due to carbon dioxide actively interacting with the PMMA functional groups [33], the diffusion of the CO₂ molecules inside the polymer matrix decreases compared to the pure fluid. Obtained data show that the diffusion coefficient of the CO₂ molecules which are located inside the PMMA sample near the ester groups is more than 10 times lower ($(2.74 \pm 0.31) \times 10^{-5} \text{ cm}^2/\text{s}$) than in bulk supercritical carbon dioxide ($(29.17 \pm 0.47) \times 10^{-5} \text{ cm}^2/\text{s}$).

Figure 9 illustrates the instant snapshots of the simulated system final configuration. To better understand the penetration process of CO₂ into the polymer we cut a 1 nm thick polymer layer from the center of the sample in three planes.

It can be seen from Figure 9 that by the end of simulation only a small part of CO₂ molecules achieved the center of the PMMA sample and solvent distribution inside the polymer is uneven. Hence, we estimate the amount of solvent sorbed by the polymer per unit mass of the polymer in two ways. First, we calculated the amount of CO₂ absorbed by PMMA taking into account not only molecules inside the polymer matrix but also molecules adsorbed on the polymer surface. The calculation was carried out as follows: the mass of carbon dioxide molecules, located at a distance of 0.35 nm from any PMMA atom was calculated for final system configuration, i.e., after 150 ns simulation. The criteria for such distance between solvent atoms and the polymer atoms was chosen based on the location of maxima on the atom-atom radial distribution functions CO₂-PMMA and average interatomic distances obtained by classical and ab initio molecular dynamics in our previous work [33]. Then we used the equation:

$$\alpha = \frac{m_{\text{CO}_2}}{m_{\text{PMMA}}} \quad (14)$$

where m_{PMMA} is the mass of the polymer and m_{CO_2} is the mass of sorbed solvent.

In the second case, we consider a few PMMA chains in the center of the polymer sample and in the same way estimate the amount of CO₂ absorbed by the polymer per unit mass of the polymer. The part of the polymer considered for calculation α is presented in Figure 10.

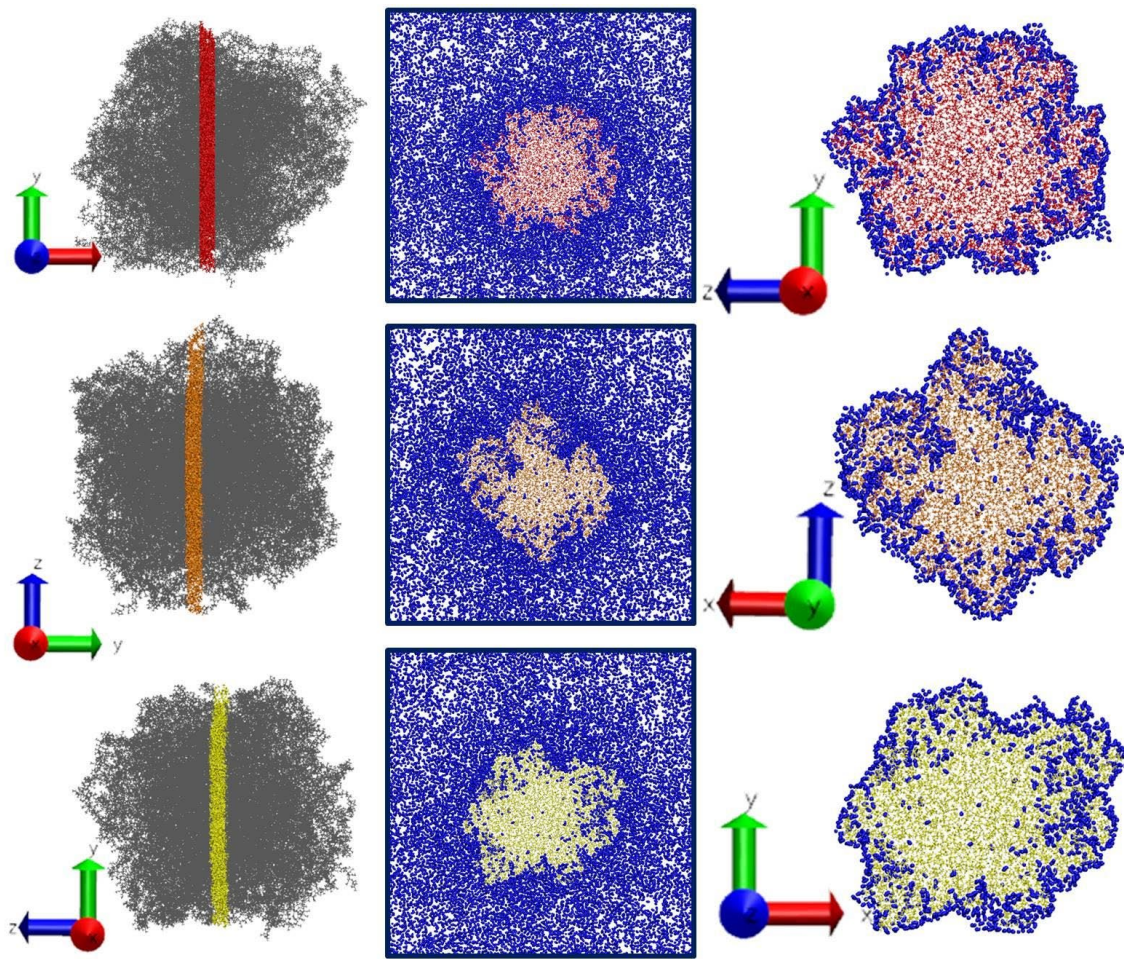


Figure 9. Instant snapshots of PMMA samples in three directions. Blue represents CO₂ molecules. The red, orange, and yellow colors in the figure represent sections of the polymer from the center of the sample in three different planes. It can be seen from the figure that some of the CO₂ molecules are not uniformly distributed in the polymer volume. The simulation results were used to further estimate the proportion of CO₂ sorbed by the PMMA polymer matrix.

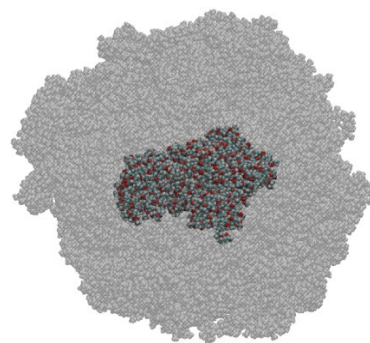


Figure 10. Snapshot of PMMA (gray) and the central part of the PMMA considered for calculation of absorbed CO₂. This snapshot shows the volume that was used to calculate the parameters of sorption according to Equation 14 at various simulation times.

The swelling degree calculated according to the first method, taking into account surface adsorption turned out to be 0.467 g/g. The amount of CO₂ absorbed by the bulk phase of the polymer is 0.118 g/g.

4. Conclusions

The work is a comprehensive study of the sorption process of supercritical carbon dioxide PMMA at 50 °C and 25 MPa by NMR spectroscopy and classical molecular dynamics. For the first time, the method based on the joint use of two approaches (2D ILT and ^{13}C NMR kinetic curve analysis) has been developed, which allows obtaining unique information about the state of CO_2 in a polymer matrix, which is a useful scientific tool for the study of such systems. In the future, this approach can be developed to control the impregnation of medicinal compounds into a polymer matrix. According to the results of the ^{13}C NMR experiment, it was found that the amount of sorbed scCO_2 on an hourly scale was 24.9%. At the same time, the total amount of sorbed CO_2 for all time according to RRCSY is 98.1%. According to the molecular dynamics data, the amount of scCO_2 sorbed by the polymer after 150 ns is 46.7%, taking into account surface adsorption. By the end of the simulation, the amount of carbon dioxide in the polymer volume was equal to 0.118 g/g. Thus, comparing the data obtained using the NMR experiment and computer modeling, we can conclude that on the second scale it is 26.5%. Much more important is that the combined use of NMR and MD modeling methods is a powerful tool for obtaining data on the sorption of CO_2 into a polymer matrix.

Supplementary Materials: The following supporting information can be downloaded at: <https://www.mdpi.com/article/10.3390/polym14235332/s1>, Figure S1: The ^{13}C NMR spectra initial time (a) and after completed (b) sorption process of CO_2 into the PMMA.

Author Contributions: Conceptualization, M.G.K.; methodology, K.V.B., A.A.D., D.L.G. and I.A.K.; software, D.L.G.; validation, K.V.B., A.A.D., I.A.K. and M.G.K.; formal analysis, K.V.B., A.A.D., D.L.G. and I.A.K.; investigation, V.V.S., K.V.B., A.A.D. and D.L.G.; resources, M.G.K.; data curation, K.V.B., A.A.D. and I.A.K.; writing—original draft preparation, V.V.S., K.V.B. and I.A.K.; writing—review and editing, V.V.S., K.V.B., A.A.D. and I.A.K.; visualization, K.V.B. and D.L.G.; supervision, I.A.K.; project administration, M.G.K.; funding acquisition, I.A.K. and M.G.K. All authors have read and agreed to the published version of the manuscript.

Funding: The research was supported by a grant of the Russian Science Foundation (project no. 22-13-00257).

Institutional Review Board Statement: Not applicable.

Data Availability Statement: Not applicable.

Conflicts of Interest: The authors declare no conflict of interest.

References

1. Anagnostakos, K.; Fürst, O.; Kelm, J. Antibiotic-Impregnated PMMA Hip Spacers: Current Status. *Acta Orthop.* **2006**, *77*, 628–637. [[CrossRef](#)] [[PubMed](#)]
2. Pantoula, M.; Panayiotou, C. Sorption and Swelling in Glassy Polymer/carbon Dioxide Systems: Part I. Sorption. *J. Supercrit. Fluids* **2006**, *37*, 254–262. [[CrossRef](#)]
3. Pantoula, M.; von Schnitzler, J.; Eggers, R.; Panayiotou, C. Sorption and Swelling in Glassy Polymer/carbon Dioxide Systems. Part II-Swelling. *J. Supercrit. Fluids* **2007**, *39*, 426–434. [[CrossRef](#)]
4. Zhang, Y.; Gangwani, K.K.; Lemert, R.M. Sorption and Swelling of Block Copolymers in the Presence of Supercritical Fluid Carbon Dioxide. *J. Supercrit. Fluids* **1997**, *11*, 115–134. [[CrossRef](#)]
5. Carla, V.; Wang, K.; Hussain, Y.; Efimenko, K.; Genzer, J.; Grant, C.; Sarti, G.C.; Carbonell, R.G.; Doghieri, F. Nonequilibrium Model for Sorption and Swelling of Bulk Glassy Polymer Films with Supercritical Carbon Dioxide. *Macromolecules* **2005**, *38*, 10299–10313. [[CrossRef](#)]
6. Van der Lee, A.; Hamon, L.; Holl, Y.; Grohens, Y. Density Profiles in Thin PMMA Supported Films Investigated by X-Ray Reflectometry. *Langmuir* **2001**, *17*, 7664–7669. [[CrossRef](#)]
7. Li, X.K.; Cao, G.P.; Chen, L.H.; Zhang, R.H.; Liu, H.L.; Shi, Y.H. Study of the Anomalous Sorption Behavior of CO_2 into Poly(methyl Methacrylate) Films in the Vicinity of the Critical Pressure and Temperature Using a Quartz Crystal Microbalance (QCM). *Langmuir* **2013**, *29*, 14089–14100. [[CrossRef](#)]
8. Aubert, J.H. Solubility of Carbon Dioxide in Polymers by the Quartz Crystal Microbalance Technique. *J. Supercrit. Fluids* **1998**, *11*, 163–172. [[CrossRef](#)]

9. Kazarian, S.G.; Chan, K.L.A. FTIR Imaging of Polymeric Materials under High-Pressure Carbon Dioxide. *Macromolecules* **2004**, *37*, 579–584. [[CrossRef](#)]
10. Ichikawa, K.; Mori, T.; Kitano, H.; Fukuda, M.; Mochizuki, A.; Tanaka, M. Fourier Transform Infrared Study on the Sorption of Water to Various Kinds of Polymer Thin Films. *J. Polym. Sci. Part B Polym. Phys.* **2001**, *39*, 2175–2182. [[CrossRef](#)]
11. Naumann, D. FT-infrared and FT-Raman spectroscopy in biomedical research. *Appl. Spectrosc. Rev.* **2001**, *36*, 239–298. [[CrossRef](#)]
12. Dubois, J.; Grau, E.; Tassaing, T.; Dumon, M. On the CO₂ Sorption and Swelling of Elastomers by Supercritical CO₂ as Studied by in Situ High Pressure FTIR Microscopy. *J. Supercrit. Fluids* **2018**, *131*, 150–156. [[CrossRef](#)]
13. Meunier, F.C. Pitfalls and Benefits of: In Situ and Operando Diffuse Reflectance FT-IR Spectroscopy (DRIFTS) Applied to Catalytic Reactions. *React. Chem. Eng.* **2016**, *1*, 134–141. [[CrossRef](#)]
14. Fried, J.R.; Li, W. High-Pressure FTIR Studies of Gas–polymer Interactions. *J. Appl. Polym. Sci.* **1990**, *41*, 1123–1131. [[CrossRef](#)]
15. Di Noto, V.; Vezzù, K.; Giffin, G.A.; Conti, F.; Bertucco, A. Effect of High Pressure CO₂ on the Structure of PMMA: A FT-IR Study. *J. Phys. Chem. B* **2011**, *115*, 13519–13525. [[CrossRef](#)]
16. Briscoe, B.J.; Lorge, O.; Wajs, A.; Dang, P. Carbon Dioxide-Poly(vinylidene Fluoride) Interactions at High Pressure. *J. Polym. Sci. Part B Polym. Phys.* **1998**, *36*, 2435–2447. [[CrossRef](#)]
17. Wissinger, R.G.; Paulaitis, M.E. Swelling and Sorption in polymer–CO₂ Mixtures at Elevated Pressures. *J. Polym. Sci. Part B Polym. Phys.* **1987**, *25*, 2497–2510. [[CrossRef](#)]
18. Keller, J.U.; Rave, H.; Staudt, R. Measurement of Gas Absorption in a Swelling Polymeric Material by a Combined Gravimetric-Dynamic Method. *Macromol. Chem. Phys.* **1999**, *200*, 2269–2275. [[CrossRef](#)]
19. Royer, J.R.; DeSimone, J.M.; Khan, S.A. Carbon Dioxide-Induced Swelling of Poly(dimethylsiloxane). *Macromolecules* **1999**, *32*, 8965–8973. [[CrossRef](#)]
20. Nikitin, L.N.; Said-Galiyev, E.E.; Vinokur, R.A.; Khokhlov, A.R.; Gallyamov, M.O.; Schaumburg, K. Poly(methyl Methacrylate) and Poly(butyl Methacrylate) Swelling in Supercritical Carbon Dioxide. *Macromolecules* **2002**, *35*, 934–940. [[CrossRef](#)]
21. Stejskal, E.O.; Schaefer, J.; Henis, J.M.S.; Tripodi, M.K. Magic-Angle Carbon-13 NMR Study of CO₂ Adsorbed on Some Molecular Sieves. *J. Chem. Phys.* **1974**, *61*, 2351–2355. [[CrossRef](#)]
22. Michael, A.; Meiler, W.; Michel, D.; Pfeifer, H. ¹³C NMR Investigations of Carbon Monoxide Adsorbed in Zeolites. *Chem. Phys. Lett.* **1981**, *84*, 30–32. [[CrossRef](#)]
23. Dardin, A.; Cain, J.B.; Desimone, J.M.; Johnson, C.S.; Samulski, E.T. High-Pressure NMR of Polymers Dissolved in Supercritical Carbon Dioxide. *Macromolecules* **1997**, *30*, 3593–3599. [[CrossRef](#)]
24. Iijima, M.; Nagasaki, Y.; Okada, T.; Kato, M.; Kataoka, K. Core-Polymerized Reactive Micelles from Heterotelechelic Amphiphilic Block Copolymers. *Macromolecules* **1999**, *32*, 1140–1146. [[CrossRef](#)]
25. Niessen, H.G.; Trautner, P.; Wiemann, S.; Bargon, J.; Woelk, K. The Toroid Cavity Autoclave for High-Pressure and Variable-Temperature in Situ Nuclear Magnetic Resonance Studies. *Rev. Sci. Instrum.* **2002**, *73*, 1259. [[CrossRef](#)]
26. Ballard, L.; Reiner, C.; Jonas, J. High-Resolution NMR Probe for Experiments at High Pressures. *J. Magn. Reson. Ser. A* **1996**, *123*, 81–86. [[CrossRef](#)]
27. Wissinger, R.G.; Paulaitis, M.E. Molecular Thermodynamic Model for Sorption and Swelling in Glassy Polymer–CO₂ Systems at Elevated Pressures. *Ind. Eng. Chem. Res.* **1991**, *30*, 842–851. [[CrossRef](#)]
28. Kamiya, Y.; Mizoguchi, K.; Terada, K.; Fujiwara, Y.; Wang, J.-S. CO₂ Sorption and Dilation of Poly(methyl Methacrylate). *Macromolecules* **1998**, *31*, 472–478. [[CrossRef](#)]
29. Rajendran, A.; Bonavoglia, B.; Forrer, N.; Storti, G.; Mazzotti, M.; Morbidelli, M. Simultaneous Measurement of Swelling and Sorption in a Supercritical CO₂-Poly(methyl Methacrylate) System. *Ind. Eng. Chem. Res.* **2005**, *44*, 2549–2560. [[CrossRef](#)]
30. Vogt, B.D.; RamachandraRao, V.S.; Gupta, R.R.; Lavery, K.A.; Francis, T.J.; Russell, T.P.; Watkins, J.J. Phase Behavior of Polystyrene-Block-Poly(n-Alkyl Methacrylate)s Dilated with Carbon Dioxide. *Macromolecules* **2003**, *36*, 4029–4036. [[CrossRef](#)]
31. Shieh, Y.-T.; Liu, K.-H. The Effect of Carbonyl Group on Sorption of CO₂ in Glassy Polymers. *J. Supercrit. Fluids* **2003**, *25*, 261–268. [[CrossRef](#)]
32. Gurina, D.L.; Budkov, Y.A.; Kiselev, M.G. Impregnation of Poly(methyl Methacrylate) with Carbamazepine in Supercritical Carbon Dioxide: Molecular Dynamics Simulation. *J. Phys. Chem. B* **2020**, *124*, 8410–8417. [[CrossRef](#)]
33. Gurina, D.; Budkov, Y.; Kiselev, M. Molecular Dynamics Study of the Swelling of Poly(methyl Methacrylate) in Supercritical Carbon Dioxide. *Materials* **2019**, *12*, 3315. [[CrossRef](#)]
34. Gurina, D.L.; Budkov, Y.A.; Kiselev, M.G. A Molecular Insight into Poly(methyl Methacrylate) Impregnation with Mefenamic Acid in Supercritical Carbon Dioxide: A Computational Simulation. *J. Mol. Liq.* **2021**, *337*, 116424. [[CrossRef](#)]
35. Kikic, I. Polymer–supercritical Fluid Interactions. *J. Supercrit. Fluids* **2009**, *47*, 458–465. [[CrossRef](#)]
36. Belov, K.V.; Dyshin, A.A.; Krestyaninov, M.A.; Efimov, S.V.; Khodov, I.A.; Kiselev, M.G. Conformational Preferences of Tolfenamic Acid in DMSO–CO₂ Solvent System by 2D NOESY. *J. Mol. Liq.* **2022**, *367*, 120481. [[CrossRef](#)]
37. Belov, K.V.; Batista de Carvalho, L.A.E.; Dyshin, A.A.; Efimov, S.V.; Khodov, I.A. The Role of Hidden Conformers in Determination of Conformational Preferences of Mefenamic Acid by NOESY Spectroscopy. *Pharmaceutics* **2022**, *14*, 2276. [[CrossRef](#)]
38. Khodov, I.A.; Belov, K.V.; Dyshin, A.A.; Krestyaninov, M.A.; Kiselev, M.G. Pressure Effect on Lidocaine Conformational Equilibria in scCO₂: A Study by 2D NOESY. *J. Mol. Liq.* **2022**, *367*, 120525. [[CrossRef](#)]
39. Khodov, I.; Dyshin, A.; Efimov, S.; Ivlev, D.; Kiselev, M. High-Pressure NMR Spectroscopy in Studies of the Conformational Composition of Small Molecules in Supercritical Carbon Dioxide. *J. Mol. Liq.* **2020**, *309*, 113113. [[CrossRef](#)]

40. Raiford, D.S.; Fisk, C.L.; Becker, E.D. Calibration of Methanol and Ethylene Glycol Nuclear Magnetic Resonance Thermometers. *Anal. Chem.* **1979**, *51*, 2050–2051. [[CrossRef](#)]
41. Shieh, Y.-T.; Liu, K.-H. Solubility of CO₂ in Glassy PMMA and PS over a Wide Pressure Range: The Effect of Carbonyl Groups. *J. Polym. Res.* **2002**, *9*, 107–113. [[CrossRef](#)]
42. Abraham, M.J.; Murtola, T.; Schulz, R.; Páll, S.; Smith, J.C.; Hess, B.; Lindahl, E. Gromacs: High Performance Molecular Simulations through Multi-Level Parallelism from Laptops to Supercomputers. *SoftwareX* **2015**, *1–2*, 19–25. [[CrossRef](#)]
43. Jorgensen, W.L.; Maxwell, D.S.; Tirado-Rives, J. Development and Testing of the OPLS All-Atom Force Field on Conformational Energetics and Properties of Organic Liquids. *J. Am. Chem. Soc.* **1996**, *118*, 11225–11236. [[CrossRef](#)]
44. Zhang, Z.; Duan, Z. An Optimized Molecular Potential for Carbon Dioxide. *J. Chem. Phys.* **2005**, *122*, 214507. [[CrossRef](#)] [[PubMed](#)]
45. Nosé, S. A Molecular Dynamics Method for Simulations in the Canonical Ensemble. *Mol. Phys.* **1984**, *52*, 255–268. [[CrossRef](#)]
46. Hoover, W.G. Canonical Dynamics: Equilibrium Phase-Space Distributions. *Phys. Rev. A* **1985**, *31*, 1695–1697. [[CrossRef](#)]
47. Parrinello, M.; Rahman, A. Polymorphic Transitions in Single Crystals: A New Molecular Dynamics Method. *J. Appl. Phys.* **1981**, *52*, 7182–7190. [[CrossRef](#)]
48. Hockney, R.W.; Goel, S.P.; Eastwood, J.W. Quiet High-Resolution Computer Models of a Plasma. *J. Comput. Phys.* **1974**, *14*, 148–158. [[CrossRef](#)]
49. Darden, T.; York, D.; Pedersen, L. Particle Mesh Ewald: An N·log(N) Method for Ewald Sums in Large Systems. *J. Chem. Phys.* **1993**, *98*, 10089–10092. [[CrossRef](#)]
50. Essmann, U.; Perera, L.; Berkowitz, M.L.; Darden, T.; Lee, H.; Pedersen, L.G. A Smooth Particle Mesh Ewald Method. *J. Chem. Phys.* **1995**, *103*, 8577–8593. [[CrossRef](#)]
51. Hess, B.; Bekker, H.; Berendsen, H.J.C.; Fraaije, J.G.E.M. LINCS: A Linear Constraint Solver for Molecular Simulations. *J. Comput. Chem.* **1997**, *18*, 1463–1472. [[CrossRef](#)]
52. Provencher, S.W. CONTIN: A General Purpose Constrained Regularization Program for Inverting Noisy Linear Algebraic and Integral Equations. *Comput. Phys. Commun.* **1982**, *27*, 229–242. [[CrossRef](#)]
53. Lee, J.H.; Labadie, C.; Springer, C.S.; Harbison, G.S.; Lee, J.H.; Labadie, C.; Springer, C.S.; Harbison, G.S. Two-Dimensional Inverse Laplace Transform NMR: Altered Relaxation Times Allow Detection of Exchange Correlation. *J. Am. Chem. Soc.* **1993**, *115*, 7761–7764. [[CrossRef](#)]
54. Caputo, P.; Loise, V.; Ashimova, S.; Teltayev, B.; Vaiana, R.; Oliviero Rossi, C. Inverse Laplace Transform (ILT) NMR: A Powerful Tool to Differentiate a Real Rejuvenator and a Softener of Aged Bitumen. *Colloids Surfaces A Physicochem. Eng. Asp.* **2019**, *574*, 154–161. [[CrossRef](#)]
55. Borgia, G.C.; Brown, R.J.S.; Fantazzini, P. Uniform-Penalty Inversion of Multiexponential Decay Data. *J. Magn. Reson.* **1998**, *132*, 65–77. [[CrossRef](#)]
56. Song, Y.Q.; Venkataramanan, L.; Hürlimann, M.D.; Flaum, M.; Frulla, P.; Straley, C. T₁-T₂ Correlation Spectra Obtained Using a Fast Two-Dimensional Laplace Inversion. *J. Magn. Reson.* **2002**, *154*, 261–268. [[CrossRef](#)]
57. Venkataramanan, L.; Song, Y.Q.; Hürlimann, M.D. Solving Fredholm Integrals of the First Kind with Tensor Product Structure in 2 and 2.5 Dimensions. *IEEE Trans. Signal Process.* **2002**, *50*, 1017–1026. [[CrossRef](#)]
58. Van Landeghem, M.; Haber, A.; D’espinoise De Lacaillerie, J.-B.; Blümich, B. Analysis of Multisite 2D Relaxation Exchange NMR. *Concepts Magn. Reson. Part A* **2010**, *36A*, 153–169. [[CrossRef](#)]
59. Dortch, R.D.; Horch, R.A.; Does, M.D. Development, Simulation, and Validation of NMR Relaxation-Based Exchange Measurements. *J. Chem. Phys.* **2009**, *131*, 164502. [[CrossRef](#)]
60. Schwartz, L.M.; Johnson, D.L.; Mitchell, J.; Chandrasekera, T.C.; Fordham, E.J. Modeling Two-Dimensional Magnetic Resonance Measurements in Coupled Pore Systems. *Phys. Rev. E—Stat. Nonlinear Soft Matter Phys.* **2013**, *88*, 032813. [[CrossRef](#)]
61. Monteilhet, L.; Korb, J.P.; Mitchell, J.; McDonald, P.J. Observation of Exchange of Micropore Water in Cement Pastes by Two-Dimensional T₂—T₂ Nuclear Magnetic Resonance Relaxometry. *Phys. Rev. E—Stat. Nonlinear Soft Matter Phys.* **2006**, *74*, 061404. [[CrossRef](#)] [[PubMed](#)]
62. McDonald, P.J.; Korb, J.P.; Mitchell, J.; Monteilhet, L. Surface Relaxation and Chemical Exchange in Hydrating Cement Pastes: A Two-Dimensional NMR Relaxation Study. *Phys. Rev. E—Stat. Nonlinear Soft Matter Phys.* **2005**, *72*, 011409. [[CrossRef](#)] [[PubMed](#)]
63. Mo, H.; Harwood, J.S.; Yang, D.; Post, C.B. A Simple Method for NMR t₁ Noise Suppression. *J. Magn. Reson.* **2017**, *276*, 43–50. [[CrossRef](#)] [[PubMed](#)]
64. McConnell, H.M. Reaction Rates by Nuclear Magnetic Resonance. *J. Chem. Phys.* **1958**, *28*, 430–431. [[CrossRef](#)]
65. Tracy, D.S.; Singh, R.P. A New Matrix Product and Its Applications in Partitioned Matrix Differentiation. *Stat. Neerl.* **1972**, *26*, 143–157. [[CrossRef](#)]
66. Liu, S. Matrix Results on the Khatri-Rao and Tracy-Singh Products. *Linear Algebra Appl.* **1999**, *289*, 267–277. [[CrossRef](#)]
67. Omi, H.; Ueda, T.; Miyakubo, K.; Eguchi, T. Dynamics of CO₂ Molecules Confined in the Micropores of Solids as Studied by ¹³C NMR. *Appl. Surf. Sci.* **2005**, *252*, 660–667. [[CrossRef](#)]
68. Nakayama, A.; Ishii, C.; Takayama, T.; Watanabe, M.; Zanma, A.; Kaneko, K.; Sugihara, K. Magnetic and Electronic Properties of Ferrocene-Doped Activated Carbon Fibers. *Synth. Met.* **1997**, *86*, 2335–2336. [[CrossRef](#)]
69. Petrakis, L. Spectral Line Shapes: Gaussian and Lorentzian Functions in Magnetic Resonance. *J. Chem. Educ.* **1967**, *44*, 432–436. [[CrossRef](#)]
70. Bleaney, B. John Hasbrouck Van Vleck, 13 March 1899—27 October 1980. *Biogr. Mem. Fellows R. Soc.* **1982**, *28*, 627–665. [[CrossRef](#)]

71. Seshadri, K.S.; Jones, R.N. The Shapes and Intensities of Infrared Absorption Bands—A Review. *Spectrochim. Acta* **1963**, *19*, 1013–1085. [[CrossRef](#)]
72. Earl, W.L.; Kim, Y.W.; Smith, D.M. NMR Measurement of Pore Structure. *Stud. Surf. Sci. Catal.* **1994**, *87*, 301–309. [[CrossRef](#)]
73. Rajabi, M.; Moradi, O.; Zare, K. Kinetics Adsorption Study of the Ethidium Bromide by Graphene Oxide as Adsorbent from Aqueous Matrices. *Int. Nano Lett.* **2017**, *7*, 35–41. [[CrossRef](#)]
74. Üzer, S.; Akman, U.; Hortaçsu, O. Polymer Swelling and Impregnation Using Supercritical CO₂: A Model-Component Study towards Producing Controlled-Release Drugs. *J. Supercrit. Fluids* **2006**, *38*, 119–128. [[CrossRef](#)]
75. D’Agostino, C.; Mitchell, J.; Mantle, M.D.; Gladden, L.F. Interpretation of NMR Relaxation as a Tool for Characterising the Adsorption Strength of Liquids inside Porous Materials. *Chem.—A Eur. J.* **2014**, *20*, 13009–13015. [[CrossRef](#)]
76. Mailhiet, S.E.; Zong, F.; Maneval, J.E.; June, R.K.; Galvosas, P.; Seymour, J.D. Quantifying NMR Relaxation Correlation and Exchange in Articular Cartilage with Time Domain Analysis. *J. Magn. Reson.* **2018**, *287*, 82–90. [[CrossRef](#)]
77. Rodts, S.; Bytchenkoff, D. Structural Properties of 2D NMR Relaxation Spectra of Diffusive Systems. *J. Magn. Reson.* **2010**, *205*, 315–318. [[CrossRef](#)]
78. Bytchenkoff, D.; Rodts, S. Structure of the Two-Dimensional Relaxation Spectra Seen within the Eigenmode Perturbation Theory and the Two-Site Exchange Model. *J. Magn. Reson.* **2011**, *208*, 4–19. [[CrossRef](#)]
79. Song, Y.Q.; Zielinski, L.; Ryu, S. Two-Dimensional NMR of Diffusion Systems. *Phys. Rev. Lett.* **2008**, *100*, 248002. [[CrossRef](#)]
80. Song, Y.Q.; Carneiro, G.; Schwartz, L.M.; Johnson, D.L. Experimental Identification of Diffusive Coupling Using 2D NMR. *Phys. Rev. Lett.* **2014**, *113*, 235503. [[CrossRef](#)]